International Journal of Minerals, Metallurgy and Materials
Volume 22, Number 11, November 2015, Page 1225
DOI: 10.1007/s12613-015-1189-5

X-ray diffraction investigation of amorphous calcium phosphate and hydroxyapatite under ultra-high hydrostatic pressure

Elisa Lam[1)], *Qinfen Gu*[2)], *Peter J. Swedlund*[1)], *Sylvie Marchesseau*[3)], *and Yacine Hemar*[1)]

1) School of Chemical Sciences, The University of Auckland, Private Bag 92019, Auckland, New Zealand

2) Australian Synchrotron, 800 Blackburn Rd., Clayton 3168, Australia

3) Université Montpellier 2, UMR IATE, Pl. E Bataillon, 34095 Montpellier cedex 5, France

(Received: 3 February 2015; revised: 14 July 2015; accepted: 14 July 2015)

Abstract: The changes in the crystal structures of synthetically prepared amorphous calcium phosphate (ACP) and hydroxyapatite (HAP) in water (1:1 mass ratio) were studied by synchrotron X-ray diffraction (XRD) under ultra-high hydrostatic pressures as high as 2.34 GPa for ACP and 4 GPa for HAP. At ambient pressure, the XRD patterns of the ACP and HAP samples in capillary tubes and their environmental scanning electron micrographs indicated amorphous and crystalline characteristics for ACP and HAP, respectively. At pressures greater than 0.25 GPa, an additional broad peak was observed in the XRD pattern of the ACP phase, indicating a partial phase transition from an amorphous phase to a new high-pressure amorphous phase. The peak areas and positions of the ACP phase, as obtained through fitting of the experimental data, indicated that the ACP exhibited increased pseudo-crystalline behavior at pressures greater than 0.96 GPa. Conversely, no structural changes were observed for the HAP phase up to the highest applied pressure of 4 GPa. For HAP, a unit-cell reduction during compression was evidenced by a reduction in both refined lattice parameters *a* and *c*. Both ACP and HAP reverted to their original structures when the pressure was fully released to ambient pressure.

Keywords: calcium phosphate; hydroxyapatite; high hydrostatic pressure; X-ray diffraction

1. Introduction

Calcium phosphates (CaPs) are complex mineral salts with high geological and biological occurrence. Geologically, they are widely distributed on the surface layer of the Earth. Biologically, they are present in normal and pathological mammalian calcifications. Normal calcifications include inorganic components of vertebrates' hard tissues such as bone and teeth, whereas pathological calcifications include atherosclerotic lesions, urinary calculi and stones, and dental calculi [1]. CaPs are also used in biomedical applications such as bone reconstruction and replacement and bone defect-filling drug carriers [2]. Furthermore, they are also present in colloidal suspensions such as milk, where they bond with phosphoproteins in casein micelles to store large amounts of calcium and inorganic phosphate in an utilizable form [3–4] and to maintain the structural integrity of the micelles [5]. Because of the importance of CaPs, the literature contains a vast range of studies related to these materials. They exhibit complex behavior because of their occurrence in different forms in nature (i.e., as orthophosphates (PO_4^{3-}), polyphosphates ($(PO_3)_n^{n-}$), and pyrophosphates ($P_2O_7^{4-}$). They can exist in amorphous or crystalline forms and have numerous compositions (different ratios of calcium/inorganic phosphate (Ca/P_i)), stabilities, and solubilities [1]. Their properties can be strongly modified by physicochemical conditions, including the Ca^{2+} and P_i concentrations, temperature, pH value, and pressure [6].

Hydroxyapatite (HAP), in particular, is a well-known form of CaP because of its existence in bone and teeth, and it is the main phosphorus source in crustal rocks [7]. HAP ($Ca_{10}(PO_4)_6(OH)_2$) (Ca/P_i ratio: 1.67) is the form of CaP that exhibits the highest stability; however, HAP also exhibits the lowest solubility [8]. In the Earth's mantle, it is stable to pressures greater than 10 GPa [9]. It exhibits a hexagonal crystal system with space group $P6_3/m$ and contains a total

Corresponding author: Elisa Lam E-mail: slam060@aucklanduni.ac.nz

of 44 atoms per unit cell [10–11]. The unit cell contains two crystallographic sites of Ca ions: columnar and screw-axis Ca. Columnar Ca ions are aligned parallel to the *c*-axis at approximate unit-cell heights of 0 and 1/2 and are linked by three shared O ions. Screw-axis Ca ions occur in two groups of three ions, with the Ca ions linked to a center OH group in the form of equilateral triangles. The triangles are orientated along the *c*-axis in the *ab* plane [11–12]. The six screw-axis Ca ions are bonded to PO_4 groups, and these PO_4 groups can be further linked to other Ca ions in the unit cell.

Amorphous calcium phosphate (ACP) ($Ca_9(PO_4)_6$) (Ca/P_i ratio: 1.5), another CaP phase, occurs most commonly in biological systems. It is a precursor phase of bone mineral in vertebrates and it may give rise to a more stable crystallized phase such as HAP under different environmental conditions [13]. In comparison to HAP, ACP exhibits amorphous characteristics and lacks any periodic distribution of atoms. It comprises an arrangement of Ca and P_i ions in clusters, known as "Posner's clusters" that exhibit S_6 symmetry. Its structure is analogous to that of HAP in that it consists of a core Ca group surrounded by another Ca group. The core is formed by a column with three Ca ions along the *c*-axis at z = 0, 1/2, and 1. At the periphery of the cluster, two groups of three Ca ions occupy positions at z = 3/4 and 1/4 [14].

Knowledge about ACP and HAP structures under the influence of hydrostatic high-pressure conditions remains limited. Hence, in the present work, we investigated the structures of ACP and HAP under the influence of high pressure by characterization using ultra-high hydrostatic pressure synchrotron X-ray diffraction (XRD) in a diamond anvil cell (DAC).

2. Materials and methods

2.1. Materials

The chemicals used include calcium nitrate (Scharlau, S.L., Spain), ammonium hydroxide, and ammonium phosphate dibasic (AJAX Finechem Pty, Ltd., Australia), all of which were analytical grade. The high-purity Milli-Q water used in the experiments exhibited resistivity of 18.2 MΩ·cm.

2.2. Preparation of ACP and HAP samples

ACP ($Ca_9(PO_4)_6$), with a Ca/P_i ratio of 1.5, was prepared on the basis of the double-decomposition method adapted from Somrani *et al.* [15]. This method required mixing two individual solutions of calcium nitrate and ammonium phosphate, followed by precipitation and then freeze drying. The calcium nitrate solution was prepared by dissolving 46.3 g of calcium nitrate ($Ca(NO_3)_2{\cdot}4H_2O$) in 0.550 L of Milli-Q water containing 40 mL of 28wt% ammonium hydroxide (NH_4OH) solution. The ammonium phosphate solution was prepared by dissolving 27.2 g of ammonium phosphate dibasic ($(NH_4)_2HPO_4$) in 1.3 L of Milli-Q water containing 40 mL of 28wt% NH_4OH solution. After these two solutions were mixed, precipitation occurred; the precipitates were immediately filtered using a Büchner funnel with mild suction. The precipitates were then washed with 3.0 L of Milli-Q water containing 15 mL of 28wt% NH_4OH solution. The filtered precipitates were subsequently frozen at –80°C in an ultra-low-temperature upright freezer and freeze dried using a FreeZone Plus 12 freeze dryer (Labconco Corp., USA), at –83°C for 72 h under a constant pressure of 0.8 Pa.

HAP ($Ca_{10}(PO_4)_6(OH)_2$), with a Ca/P_i ratio of 1.67, was prepared according to the method of Jarcho *et al*. [16]. This synthesis involved inducing precipitation through mixing 1 mol/L $Ca(NO_3)_2{\cdot}4H_2O$ and 0.6 mol/L $(NH_4)_2HPO_4$ solutions. The $Ca(NO_3)_2{\cdot}4H_2O$ solution was prepared by dissolving 43.15 g of $Ca(NO_3)_2{\cdot}4H_2O$ in 90 mL of Milli-Q water. The pH of this solution was adjusted to 11 using concentrated NH_4OH (~4 mL) and then further diluted with Milli-Q water to a final volume of 180 mL. The $(NH_4)_2HPO_4$ solution was prepared by dissolving 25.87 g of $(NH_4)_2HPO_4$ in 150 mL of Milli-Q water. Similar to preparation of the $Ca(NO_3)_2{\cdot}4H_2O$ solution, the pH of the $(NH_4)_2HPO_4$ solution was also adjusted to 11 using concentrated NH_4OH (~80 mL) and then further diluted with Milli-Q water to a final volume of 320 mL. The $(NH_4)_2HPO_4$ solution was added dropwise to the $Ca(NO_3)_2{\cdot}4H_2O$ solution over a period of 30 to 40 min at room temperature and under vigorous stirring. The resultant precipitate was milky and relatively gelatinous. To ensure complete formation of HAP, the system was stirred at room temperature for an additional 24 h. The aged suspension was centrifuged at 632 × *g* for 10 min at 25°C using a Heraeus centrifuge (Labofuge 400, Thermo Scientific, Germany). The precipitates were collected, washed thoroughly with Milli-Q water, and further re-centrifuged under the same conditions using the same centrifuge. The resultant white sludge was suspended in Milli-Q water, and the solids present were recovered under filtration using a Büchner funnel with mild suction for 3 h. After filtration, an adhesive, compacted filter cake was obtained. This filter cake was subsequently dried at 90°C for 15 h to yield the final HAP compact material.

ACP and HAP aqueous suspensions for high-pressure XRD were prepared by mixing ACP and HAP powders prepared with Milli-Q water in a 1:1 mass ratio.

2.3. Environmental scanning electron microscopy

Environmental scanning electron microscopy (ESEM) was used to characterize the morphology and crystalline properties of ACP and HAP. The samples were mounted onto black carbon tape and subsequently sputter-coated with a double layer of platinum using a Q150 RS rotary-pumped sputter-coating system (Quorum Technologies Ltd., UK) for 15 min. The sputter-coating system was operated at a chamber pressure of 10 Pa and a current of 20 mA. Imaging was performed using an environmental scanning electron microscope (FEI Quanta 200F, USA) equipped with a large-field detector (LFD); the microscope was operated at a pressure of 77.3 Pa and in the voltage range between 10.0 and 20.0 kV.

2.4. High-pressure X-ray diffraction

The high-pressure XRD experiments were performed on the Powder Diffraction (PD) beamline at the Australian Synchrotron (Melbourne, Australia). The experimental data were collected using monochromatic X-rays at a wavelength of 0.0688 nm. XRD measurements were performed on synthetically prepared ACP and HAP powdered samples in a capillary, followed by ACP and HAP aqueous suspensions in a DAC under ultra-high hydrostatic pressure at room temperature (approximately 23°C). The detector used for collecting the CaP powder capillary data was a Mythen-II detector, whereas that used for collecting pressure-treated liquid CaP data was a MarCCD 165 detector.

The high-pressure XRD experiment was conducted with a DAC (easyLab, UK) with 0.8-mm-culet-size diamond anvils and a rhenium gasket (preindented to 0.1 mm). A 0.3-mm hole was drilled into the setup using a Boehler micro driller (easyLab, UK) to hold the ACP and HAP liquid samples while pressure was applied. Ruby balls were loaded with the samples to measure the exact internal pressure. The pressure was measured on the basis of the shift of the ruby fluorescence, as determined using an Optiprexx Ruby Lux system (easyLab, UK). During all XRD measurements, the diffraction patterns were recorded at 20 s per cycle and were multi-read 30 times in a total run time of 10 min. All measurements were performed under room-temperature conditions, and all data were analyzed using the TOPAS V4.2 software.

3. Results and discussion

Prior to performing high-pressure XRD measurements on ACP and HAP liquid samples, we investigated the crystallinity and phases of the ACP and HAP powdered samples in capillaries at atmospheric pressure through their diffraction patterns (results not shown). The diffraction pattern of ACP contained only a broad and poorly defined diffraction peak at $2\theta \approx 13°$. The absence of sharp peaks, in agreement with the results presented by Cross *et al.* [17] and Combes and Rey [14], indicates that ACP lacked crystalline characteristics. Conversely, HAP exhibited numerous sharp diffraction peaks, indicating that its structure exhibited crystalline characteristics, and is in agreement with the reported crystal structure for this compound. The HAP diffraction pattern matched the HAP data obtained from the International Centre for Diffraction Data (ICDD) PDF–4+2013 database. The surface morphology and crystalline properties of ACP and HAP were further characterized by ESEM; the resulting micrographs are displayed in Fig. 1. The ACP sample was composed of densely packed spheres, although crystals were not discernible; in contrast, HAP contained crystals with an agglomerated structure.

The XRD patterns of ACP liquid samples subjected to various pressures ranging from 0 to 2.34 GPa are shown in Fig. 2(a). At atmospheric pressure (0 GPa), the pattern of ACP contained only a broad diffraction peak at $2\theta \approx 13.64°$ (designated as peak 1 in Fig. 2(a)). This broad diffraction peak of ACP is characteristic of an amorphous state. The absence of sharp peaks indicates that ACP lacks long-range periodicity, which is an important feature of the crystalline state [18]. This result is consistent with those of Posner and Betts [19], Combes and Rey [14], and Rabadjieva *et al.* [20], who reported that ACP exhibits amorphous characteristics, as indicated by the presence of a broad peak in its XRD pattern. When the pressure was increased from 0.25 to 2.34 GPa, an additional peak at $2\theta \approx 10°$ (designated as peak 2 in Fig. 2(a)) appeared. This additional peak signifies the formation of a new high-pressure amorphous phase. The high-pressure amorphous–amorphous transition is due to the variation in the interbond angles and interatomic distances in the material [21–22]. These variations alter the range of interatomic distances and transform the coordination of the atoms [23], resulting in poly-amorphism, i.e., a structural transition between two amorphous phases. Peak 1 was observed under all of the investigated pressure conditions; however, its peak area and position changed with pressure. The same behavior was observed in the case of peak 2 for pressures between 0.25 and 2.34 GPa. To better demonstrate the change in peak area and peak position, we plotted the peak areas and positions as functions of pressure in Figs. 2(b) and 2(c), respectively. The peak areas and positions were acquired by fitting the backgrounds of the diffraction patterns in Fig. 2(a) with a third-order Chebychev function

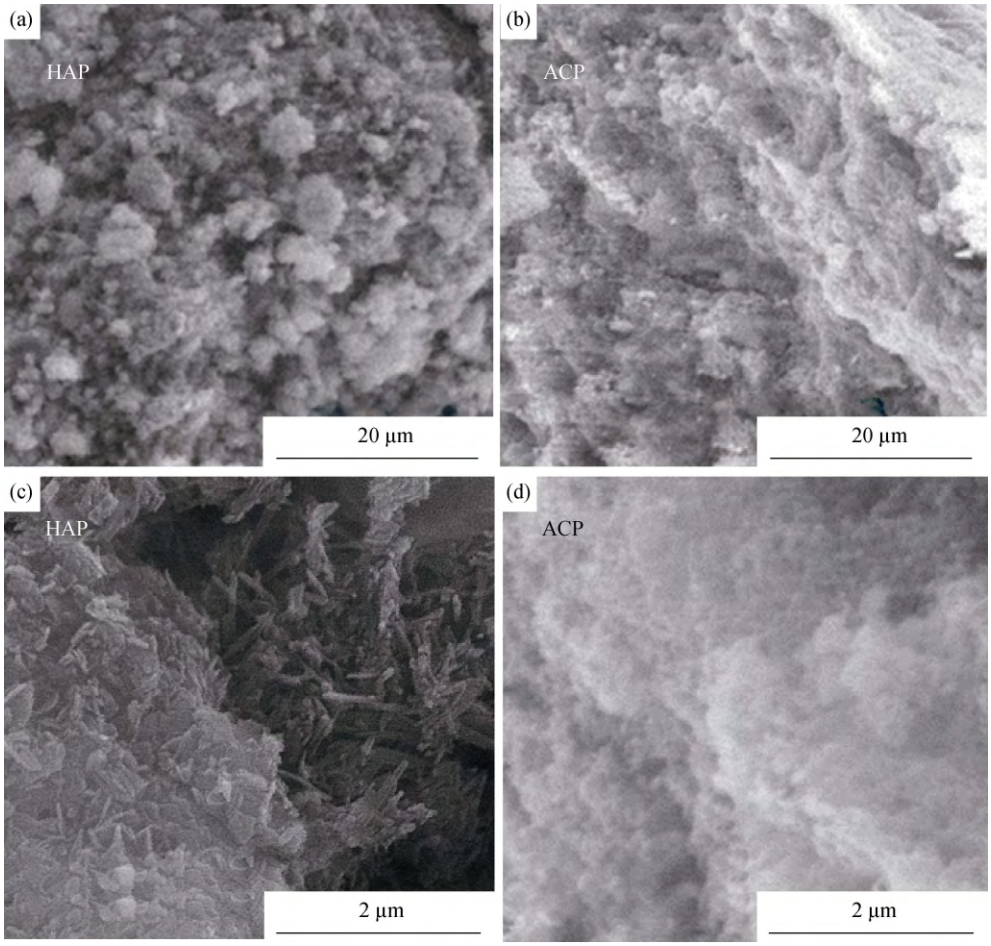

Fig. 1. ESEM micrographs of ACP and HAP.

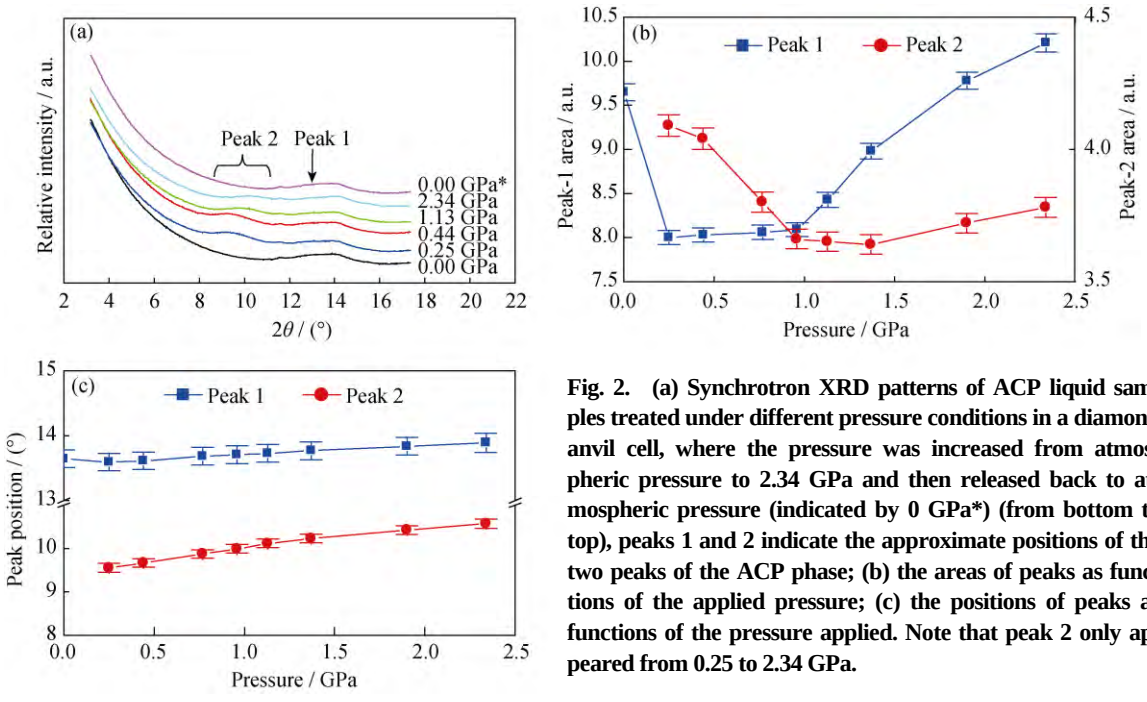

Fig. 2. (a) Synchrotron XRD patterns of ACP liquid samples treated under different pressure conditions in a diamond anvil cell, where the pressure was increased from atmospheric pressure to 2.34 GPa and then released back to atmospheric pressure (indicated by 0 GPa*) (from bottom to top), peaks 1 and 2 indicate the approximate positions of the two peaks of the ACP phase; (b) the areas of peaks as functions of the applied pressure; (c) the positions of peaks as functions of the pressure applied. Note that peak 2 only appeared from 0.25 to 2.34 GPa.

and subsequently fitting the peak area using mixed Gaussian and Lorentzian functions. The area of peak 1 at atmospheric pressure was 9.65 ± 0.10 (Fig. 2(b)). When the pressure was increased to 0.25 GPa, the peak-1 area decreased to 8.00 ± 0.08 and peak 2 appeared. The appearance of peak 2 in conjunction with the decreased peak-1 area indicates a partial phase transition from the ambient-pressure amorphous phase to a new high-pressure amorphous phase. At pressures between 0.25 and 0.96 GPa, the peak-1 area remained nearly constant, indicating that the remaining ambient-pressure amorphous ACP phase was apparently stable in this pressure range; in contrast, the peak-2 area slightly decreased, indicating a decrease in crystallinity of the new high-pressure phase. However, at pressures between 0.96 and 2.5 GPa (the highest pressure applied), both peak areas increased, indicating an increase in the pseudo-crystalline behavior of both amorphous phases. Both peaks (1 and 2) continuously shifted to larger 2θ angles as the pressure was increased (Fig. 2(c)), indicating that the interatomic distances of ACP decreased as both phases were compressed. During compression, the packing density increased continuously. The new high-pressure phase (peak 2) exhibits compressibility similar to that of the ambient-pressure phase (peak 1). When the pressure was decreased to ambient pressure (shown by 0 GPa* in Fig. 2(a)) after a pressure of 2.34 GPa had been applied, the XRD pattern was almost identical to that before compression. This similarity indicates that the ACP phase transition at pressures above 0.25 GPa is reversible.

The X-ray diffractograms of HAP samples subjected to high pressures ranging from 0 to 4 GPa are presented in Fig. 3(a). The XRD data for the HAP phase at different pressures gave similar diffraction patterns, with the peaks shifted to higher 2θ angles, indicating that no structural changes occurred under the applied pressure conditions. The data for the calcium phosphate hydroxide ($Ca_5(PO_4)_3(OH)$) hexagonal phase (space group: $P6_3/m$ (176)) in the ICDD PDF–4+2013 database were used as the starting values for Lebail refinement of the pressure-treated HAP data using the TOPAS V4.2 software. The refined lattice parameters a and c of the HAP phase as a function of pressure are shown in Fig. 3(b). The XRD data of the HAP phase revealed its unit-cell dimensions at ambient pressure to be a = (0.935 ± 0.009) nm and c = (0.686 ± 0.007) nm. These results are similar to the results of previous studies by Brunet *et al.* [7] and Kay *et al.* [24]. The lattice parameters a and c decreased continuously with increasing pressure (Fig. 3(b)), reaching (0.912 ± 0.009) nm and (0.675 ± 0.007) nm, respectively, at 4.00 GPa. The compressibility of the individual a and c parameters differed, with the unit cell being more compressible along the a-axis. This result is also in agreement with the results presented by Brunet *et al.* [7]. By using the refined lattice parameters a and c, we calculated the volume of the unit cell (V) for the hexagonal crystal system according to the equation

$$V = a^2 c \sin 60° \tag{1}$$

The results are plotted as a function of pressure in Fig. 3(c). The V at atmospheric pressure was (0.520 ± 0.005) nm^3. Similar to ACP samples, when the pressure was fully released and the system returned to atmospheric pressure, the unit-cell parameters of the HAP phase reverted to its their original values.

To model the experimental volume–pressure data, we used the second- and third-order Birch–Murnaghan equations. Unfortunately, neither of these equations could yield a good agreement with the data over the entire pressure range because of the high-pressure isostructural phase transition. To remedy this drawback, we used the second-order Birch–Murnaghan equation of state (EoS) [25] implemented in the Origin software to fit two regions of the volume–pressure curve:

$$P = \frac{3}{2} B_0 \left[\left(\frac{V}{V_0} \right)^{-\frac{7}{3}} - \left(\frac{V}{V_0} \right)^{-\frac{5}{3}} \right] \tag{2}$$

where P is the pressure, B_0 is the bulk modulus of HAP at ambient P, and V and V_0 are the unit-cell volumes at P and ambient P, respectively. The fitting results are shown as solid and dashed lines in Fig. 3(c). At low applied pressures (P < 1.5 GPa), the fitting resulted in B_0 = (35.2 ± 1.9) GPa and V_0 = (0.519 ± 0.001) nm^3; at higher pressures (P > 1.5 GPa), values of (91.4 ± 6.7) GPa and (0.506 ± 0.001) nm^3 were determined for B_0 and V_0, respectively. This latter bulk modulus and the former unit-cell volume are similar to the values previously reported by Brunet *et al.* [7] (i.e., B_0 = (97.5 ± 1.8) GPa and V_0 = (0.527 ± 0.001) nm^3). Notably, the volume–pressure data and its fitting reported by Brunet *et al.* [7] are for HAP in ethanol. Conceivably, differences may exist in the crystal shape, size, and internal stain of the HAP used in the present study and that used in the study of Brunet *et al.* [7]. A possible reason for the greater compressibility for HAP at low pressures in the present study is the use of water as a pressure-transmitting medium instead of ethanol. Water has a more open structure; thus, water–water interactions among the water molecules surrounding the HAP molecules would have a less compact spatial arrangement than in a system containing ethanol molecules, leading to a greater compressibility in the case of an aqueous system under pressure.

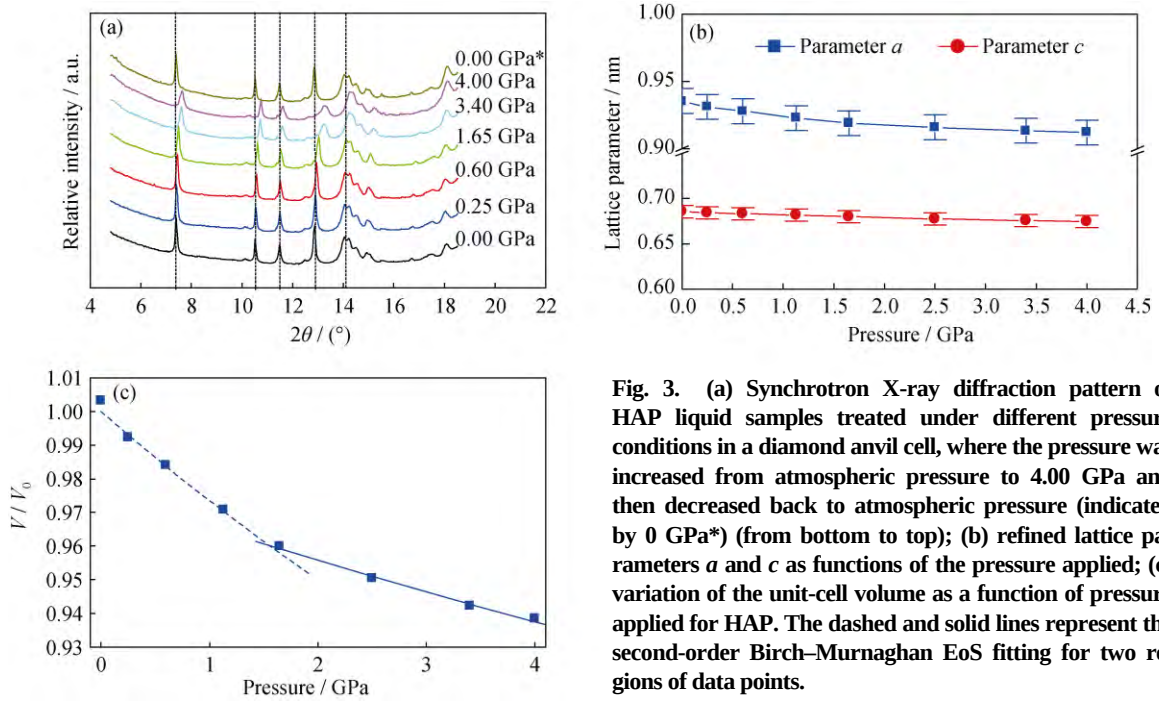

Fig. 3. (a) Synchrotron X-ray diffraction pattern of HAP liquid samples treated under different pressure conditions in a diamond anvil cell, where the pressure was increased from atmospheric pressure to 4.00 GPa and then decreased back to atmospheric pressure (indicated by 0 GPa*) (from bottom to top); (b) refined lattice parameters *a* and *c* as functions of the pressure applied; (c) variation of the unit-cell volume as a function of pressure applied for HAP. The dashed and solid lines represent the second-order Birch–Murnaghan EoS fitting for two regions of data points.

4. Conclusions

At ambient pressure, XRD and ESEM results for the ACP and HAP phases demonstrated that these materials exhibit amorphous and crystalline characteristics, respectively. When the pressure was increased to 2.34 GPa, ACP underwent partial phase transitions to a new high-pressure amorphous phase, as indicated by the appearance of a new peak in its XRD pattern. At pressure greater than 0.96 GPa, ACP exhibited increased pseudo-crystalline behavior, as evident by the increase in the peak areas of both peaks. When the pressure was fully relieved after the highest pressure (2.34 GPa) was applied, the ACP phase transition was reversible. With respect to HAP, no structural changes were observed under the pressure conditions investigated in this work. The unit-cell volume decreased as the material was compressed, as indicated by the reduction of the refined lattice parameters *a* and *c*. Similar to ACP, HAP reverted to its original unit-cell volume when the pressure was fully relieved to atmospheric pressure. The results of this study can assist in further understanding the potential of high pressure in inducing the structural transition of ACP as a precursor phase to a more crystalline phase such as HAP in bone mineral. Further, the results can also indirectly provide a deeper understanding of the structural changes of CaPs in pressure-treated milks for the dairy industry.

Acknowledgements

We would like to thank Martha Arifin for preparation of the synthetic ACP and HAP powders. This work is funded through an FRDF funding (Grant 3702239) provided by the University of Auckland, New Zealand. Part of this research was undertaken on the Powder Diffraction beamline at the Australian Synchrotron, Melbourne, Australia.

References

[1] S.V. Dorozhkin and M. Epple, Biological and medical significance of calcium phosphates, *Angew. Chem. Int. Ed.*, 41(2002), No. 17, p. 3130.

[2] S.M. Zhai and X. Wu, X-ray diffraction study of β-$Ca_3(PO4)_2$ at high pressure, *Solid State Commun.*, 150(2010), No. 9-10, p. 443.

[3] C. Holt and R. Jenness, Interrelationships of constituents and partition of salts in milk samples from eight species, *Comp. Biochem. Physiol. Part A*, 77(1984), No. 2, p. 275.

[4] T.C.A. McGann, R.D. Kearney, W. Buchheim, A.S. Posner, F. Betts, and N.C. Blumenthal, Amorphous calcium phosphate in casein micelles of bovine milk, *Calcif. Tissue Int.*, 35(1983), p. 821.

[5] R. Jenness, *Fundamentals of Dairy Chemistry*, Springer US, New York, 1988, p. 1.

[6] F. Gaucheron, Calcium phosphates in dairy products, [in] *Calcium Phosphate*: *Structure*, *Synthesis*, *Properties and Applications*, Edited by R.B Heimann, Nova Science Publishers,

Inc., New York, 2012, p. 381.

[7] F. Brunet, D.R. Allan, S.A.T. Redfern, R.J. Angel, R. Miletich, H.J. Reichmann, J. Sergent, and M. Hanfland, Compressibility and thermal expansivity of synthetic apatites, $Ca_5(PO_4)_3X$ with X = OH, F and Cl, *Eur. J. Mineral.*, 11(1999), No. 6, p. 1023.

[8] B. Mirhadi, B. Mehdikhani, and N. Askari, Synthesis of nano-sized β-tricalcium phosphate via wet precipitation, *Process. Appl. Ceram*., 5(2011), No. 4, p. 193.

[9] A.E. Beswick and I.S.E. Carmichael, Constraints on mantle source compositions imposed by phosphorus and the rare-earth elements, *Contrib. Mineral. Petrol*., 67(1978), No. 3, p. 317.

[10] A. Mortier, J. Lemaitre, L. Rodrique, and P.G. Rouxhet, Synthesis and thermal behavior of well-crystallized calcium-deficient phosphate apatite, *J. Solid State Chem*., 78(1989), No. 2, p. 215.

[11] M. Corno, R. Orlando, B. Civalleri, and P. Ugliengo, Periodic B3LYP study of hydroxyapatite (001) surface modelled by thin layer slabs, *Eur. J. Mineral.*, 19(2007), No. 5, p. 757.

[12] J. Jeanjean, U. Vincent, and M. Fedoroff, Structural modification of calcium hydroxyapatite induced by sorption of cadmium ions*, J. Solid State Chem*., 108(1994), No. 1, p. 68.

[13] E.D. Eanes, Amorphous calcium phosphate: Thermodynamic and kinetic considerations, [in] *Calcium Phosphates in Biological and Industrial Systems*, Edited by Z. Amjad, Kluwer Academic Publishers, Massachusetts, 1998, p. 21.

[14] C. Combes and C. Rey, Amorphous calcium phosphates: Synthesis, properties and uses in biomaterials, *Acta Biomater.*, 6(2010), No. 9, p. 3362.

[15] S. Somrani, M. Banu, M. Jemal, and C. Rey, Physico-chemical and thermochemical studies of the hydrolytic conversion of amorphous tricalcium phosphate into apatite, *J. Solid State Chem*., 178(2005), No. 5, p. 1337.

[16] M. Jarcho, C.H. Bolen, M.B. Thomas, J. Bobick, J.F. Kay, and R.H. Doremus, Hydroxylapatite synthesis and characterization in dense polycrystalline form, *J. Mater. Sci*., 11(1976), No. 11, p. 2027.

[17] K.J. Cross, N.L. Huq, J.E. Palamara, J.W. Perich, and E.C. Reynolds, Physicochemical characterisation of casein phosphopeptide-amorphous calcium phosphate nanocomplexes, *J. Biol. Chem*., 280(2005), No. 15, p. 15362.

[18] J.D. Termine and E.D. Eanes, Comparative chemistry of amorphous and apatitic calcium phosphate preparations, *Calcif. Tissue Res.*, 10(1972), No. 1, p. 171.

[19] A.S. Posner and F. Betts, Synthetic amorphous calcium phosphate and its relation to bone mineral structure, *Acc. Chem. Res*., 8(1975), No. 8, p. 273.

[20] D. Rabadjieva, R. Gergulova, R. Titorenkova, S. Tepavitcharova, E. Dyulgerova, C. Balarew, and O. Petrov, Biomimetic transformations of amorphous calcium phosphate: Kinetic and thermodynamic studies, *J. Mater. Sci. Mater. Med*., 21(2010), No. 9, p. 2501.

[21] R.J. Hemley and H.K. Mao, Static high-pressure effects in solids, [in] *Encyclopedia of Applied Physics*, Vol. 18, Edited by G.L. Trigg, E.S. Vera and W. Greulich, VCH Publishers, New York, 1997, p. 555-572.

[22] R.J. Hemley and N.W. Ashcroft, The revealing role of pressure in the condensed matter sciences, *Phys. Today*, 51(1998), No. 8, p. 26.

[23] T. Loerting, V.V. Brazhkin, and T. Morishita, Multiple amorphous-amorphous transitions, *Adv. Chem. Phys*., 143(2009), p. 29.

[24] M.I. Kay, R.A. Young, and A.S. Posner, Crystal structure of hydroxyapatite, *Nature*, 204(1964), No. 496, p. 1050.

[25] F. Birch, Finite elastic strain of cubic crystals, *Phys. Rev.*, 71(1947), No. 11, p. 809.